Meshing strategy for movable control surfaces: towards high-fidelity flight maneuver simulations

Larissa Bruna Streher[1,2] and Ralf Heinrich[1]

[1] Deutsches Zentrum für Luft- und Raumfahrt, Institute of Aerodynamics and Flow Technology, Lilienthalplatz 7, 38108 Braunschweig, Germany,
[2] University of Groningen, Bernoulli Institute for Mathematics, Computer Science and Artificial Intelligence, Nijenborgh 9, 9747 AG Groningen, The Netherlands,
{larissa.streher;ralf.heinrich}@dlr.de

Abstract High-fidelity flight maneuver simulations are crucial for the development of realistic digital aircraft models. However, such simulations are still hampered by difficulties in modeling the relative body motion between control and lifting surfaces when using realistic configurations. The presence of spanwise gaps between lifting and control surfaces impedes the application of concepts such as mesh deformation, and hampers the usage of mesh deformation combined with the overset method since the mesh generation process is particularly cumbersome. To reduce the user effort to create overset meshes, we have developed a methodology to automatically create overlapping regions for matching block interfaces. Hence, the usage of the overset method combined with mesh deformation for modeling moving control surfaces is facilitated, and a significant advance towards the computation of high-fidelity flight maneuvers is achieved.

Keywords: CFD · Mesh generation · Control surface modeling

1 Introduction

Aircraft control surfaces are movable aerodynamic devices designed to maintain the aircraft stable, and yet responsive to any control surface deployment. The deflection of such surfaces changes the aerodynamic forces and moments acting on the aircraft and are, therefore, used for trimming and maneuvering purposes. The accurate prediction of the flow around maneuvering aircraft is of major importance for the development of realistic digital models of aircraft, which would enable a reduction of time and costs involved in the design and certification of aircraft [5]. The simulation of high-fidelity flight maneuvers throughout the entire flight envelope is, however, still hampered due to difficulties in the dynamical modeling of movable control surfaces.

Many approaches for modeling moving control surfaces have already been proposed, such as mesh regeneration, mesh deformation, and combinations of overset (Chimera) grids with either rigid body rotation or mesh deformation [3]. Mesh regeneration consists of generating new high-quality meshes for each deflection angle of the control surfaces. This alternative is, however, very time

consuming and only suitable for steady control surface deflections since it does not preserve the mesh connectivity. Mesh deformation, in contrast, deforms the mesh to fit the new configuration without modifying the grid connectivity and is, therefore, suitable for steady and unsteady control surface deflections. This approach is, however, not capable of modeling the spanwise gaps present between the lifting and control surfaces, since highly sheared grid elements appear in the gap region already at low deflection angles [6]. The combination of overset meshes with rigid body rotation, on the other hand, is capable of modeling the spanwise gaps, but also requires the introduction of a streamwise gap. Albeit such a gap is usually present in real configurations, it is normally sealed. Thus, a wing configuration that considers the streamwise gap is usually not realistic and therefore not suitable for high-fidelity simulations. Conversely, the combination of Chimera meshes with mesh deformation enables the usage of realistic wing configurations without changing the mesh connectivity for each deflection angle. This approach is, therefore, applied in this work.

The combination of overset meshes with mesh deformation is based on the creation of overset grid blocks for the control surfaces, which are deployed through mesh deformation algorithms. Although this approach has been successfully tested, e.g., by Reimer and Heinrich [7], it has a major drawback: the process of generating valid, high-quality Chimera meshes is cumbersome (especially for the narrow gap regions) and time consuming.

Aiming at reducing the user effort required to generate high-quality overset meshes, we have developed a methodology that extends matching block interfaces. This methodology has been implemented on an add-on of the finite volume software DLR TAU [9], yielding the so-called *AutoLap* software. With *AutoLap*, overlapping regions with user-defined number of cell layers can, then, be easily and automatically generated for TAU mesh files based on the NetCDF interface [8]. Thereby, computations of aircraft with movable control surfaces using the overset method combined with mesh deformation are facilitated.

2 Automatic overlapping region generation for matching block interfaces: The *AutoLap* software

The *AutoLap* software is based on the idea of Blades and Marcum [2]: extruding the faces along the grid block interface into the adjacent subdomain based on information of this subdomain. Here, we apply this idea exclusively to blocks that have matching interfaces, i.e., when the element faces and nodes on the interfaces of both subdomains are located at the same place. Consequently, elements on the adjacent subdomain can be simply added to the connectivity list of the grid block being considered.

As a starting point for *AutoLap*, a multi-block grid with matching block interfaces is to be imported into the software. The user then defines the number of cell layers to be added either to a specific matching interface or to all available matching interfaces. Next, *AutoLap* identifies the matching interface pairs of the input grid using bounding boxes that enclose all points of each bound-

ary previously defined as a matching interface. If the definition of bounding boxes is not sufficient to determine the interface pairs, arbitrary points on the considered interface are tested to determine whether there is a point located on the same position that lies on the candidate interface pair and, if needed, on other matching interfaces or on the grid block of the candidate interface pair.

Once the matching interface pairs are defined, the layers of elements that are to be added to the (target) interface can be identified and flagged based on the neighboring elements of the partner (donor) interface elements. First, the points on the target matching interface are located and the corresponding donor points, i.e., points that are located at the same position as the target points but are part of the donor grid block, are flagged. The donor points are, then, divided into so-called *Chimera* and *non-Chimera points*. The former are the points that are connected to any Chimera boundary (on either the target or the donor grid block), or the points that are no longer on both partner matching interfaces. The latter, i.e., the *non-Chimera points*, are the points that do not meet the criteria to be *Chimera* points.

With the flagged points divided into *Chimera* and *non-Chimera points*, the volume elements can be flagged. All volume elements connected to the *non-Chimera points* are flagged, as these elements are never present on the target grid block. For the *Chimera points*, the flagging process is carried out carefully in order to avoid the generation of duplicate elements. First, all volume elements connected to the donor *Chimera points* that were not already flagged with the *non-Chimera points* are identified, and the underlying donor points are further separated into so-called *valid* and *invalid* (donor) *points*. The *valid points* are either those that have no corresponding points on the target grid block, or those that have such corresponding points and meet the following criteria: they do not lie on a Chimera boundary on the donor grid block, or they lie on such a boundary, provided that they simultaneously lie on a matching interface on the donor block, or their corresponding target point belongs to a Chimera surface on the target block. The *invalid points* are those that do not meet the criteria to be considered *valid points*. If the previously identified donor element consists exclusively of *valid points* that are not located on domain boundaries, it is directly flagged. Otherwise, the element is only flagged if it is not already present on the target grid block.

Finally, the faces of all previously flagged volume elements are analyzed in order to accommodate the extended boundary. If the face is connected to a volume element, *AutoLap* first verifies whether a corresponding surface element is available on the target grid block. In case such a surface is indeed available, the surface element on the target block is marked for later deletion as the underlying boundary is shifted by one cell layer. Otherwise, the points constituting the face are stored and the new surface element, which accommodates the shifted boundary, is flagged. In case the considered face is connected to a surface element, *AutoLap* verifies whether this element is located on a matching interface with the target block. If the surface element does not lie on such an interface, it is flagged in order to accommodate the new boundary. Otherwise, the donor surface element

is tagged for a later change of the boundary type to Chimera, whereas the corresponding target surface element, if available, is marked for later deletion.

If the specified matching interface must be extended by more than one cell layer, the entire flagging process is repeated until the user-defined number of cell layers is marked. In case the cell layer being flagged is not the first one, the point flagging process that forms the basis for the volume element search is, however, based on the surface elements marked on the previously flagged layer.

As soon as the flagging process is completed, the flagged elements can be added to the target grid block. First, the points that are not present on the target grid block and that are required to construct the flagged elements, are created at the same location as the underlying donor points. Second, volume elements that are topologically the same as the flagged ones are generated. Next, the surface elements that have been flagged for deletion are removed from the grid connectivity. Subsequently, the surface elements flagged on the last cell layer are created. Finally, the boundary type of the newly created elements is set to Chimera, and the boundary type of the donor surface elements that were flagged for later modification are updated to Chimera as well. The overlapping region is, then, successfully created for the specified matching interface. If the partner matching interface or other matching interfaces are also to be treated, the same process is to be applied, bearing in mind that the input grid for the former is the grid with the original matching interface and for the latter the grid with the extended patched surface. If no further matching interfaces are to be treated, the grid with the automatically generated overlapping region can be written and used for CFD simulations with the overset meshes technique.

3 Test cases

AutoLap is tested here for three different test cases. First, the solution of a Prandtl-Meyer expansion fan is computed for single-block reference grids and two-block Chimera grids, which overlapping regions are generated by *AutoLap*. The solution obtained with all grids are compared, ensuring that the overlapping region was successfully created. Next, a test case in which a Chimera boundary of the expansion fan slides in the stream-wise direction according to a sinusoidal function is investigated. The grid is gradually deformed and the concept that we aim to apply to control surfaces, i.e., mesh deformation combined with overset meshes with automatically generated overlapping regions, is proven. Finally, the deflection of an arbitrary aileron of a NACA wing is tested for a reference grid fully generated by a mesh generation software and a grid in which the overlapping region in the gaps between control and lifting surfaces are generated with the *AutoLap* software. The results are compared and the applicability of *AutoLap* for realistic configurations with moving control surfaces is verified.

All computations are carried out with the cell-vertex DLR TAU Code [9]. The governing equations are discretized in space with a second-order accurate finite volume method. The convection term is discretized with a second-order accurate central scheme with added Matrix dissipation. To deform the meshes,

surface deflections are prescribed and a thin plate spline[4] is used to interpolate the deflections into the volume grid.

3.1 Prandtl-Meyer expansion fan

Here, we investigate the supersonic flow of air about a concave corner, which leads to the so-called Prandtl-Meyer expansion fan. The flow is herein considered inviscid and has the following free-stream properties: pressure of $p_\infty = 101325\,\text{Pa}$, temperature of $T_\infty = 273.15\,\text{K}$, and Mach number of $Ma_\infty = 1.5$. The two-dimensional expansion fan geometry is characterized by a turn angle of $\theta = 7.6°$, an inlet height of $H_\text{in} = 2.3\,\text{m}$, an outlet height of $H_\text{out} = 2.5\,\text{m}$, and a width of $L_\text{x} = 2\,\text{m}$, whereby the expansion corner lies at $0.25\,L_\text{x}$.

Two single-block reference grids are first generated for the above described geometry: *ref. structured* (single-block structured grid with 6954 mesh nodes) and *ref. unstructured* (single-block unstructured grid with 9662 grid nodes). In addition to the reference grids, two other two-block grids are created with the matching interface located at $z_\text{int} = 0.3\,\text{m}$, as illustrated in Fig. 1. Overlapping regions consisting of two cell layers for the multi-block grids are, then, automatically generated by the *AutoLap* software and two Chimera grids are obtained: *Chim. structured* with 7564 mesh nodes, and *Chim. unstructured* with 10278 mesh nodes. Except from the overlapping region and the grid block structure, these overset meshes are essentially the same as the reference grids (see Fig. 1).

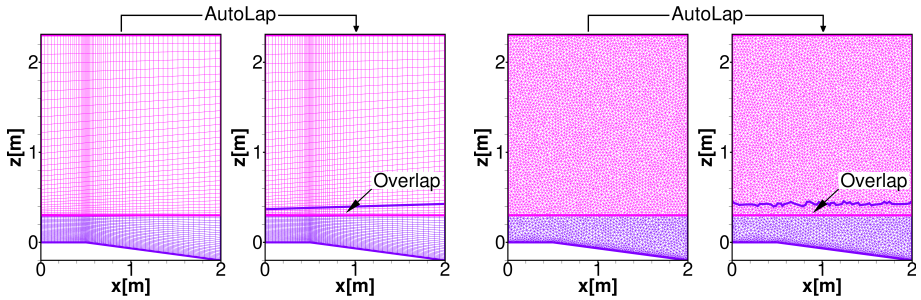

(a) Structured grid. (b) Unstructured grid.

Figure 1: Expansion fan grid before (left) and after (right) the generation of overlapping regions with *AutoLap*. The bottom and top grid blocks are depicted in purple and pink, respectively.

Steady-state test case. The steady-state solution of the expansion fan is computed with the reference and Chimera grids. As expected, donor cells are found for all Chimera interpolation points. Figure 2 shows the Mach number distribution for the reference and Chimera grids, as well as the location of the forward and rearward Mach lines obtained with the inviscid compressible flow theory (analytical solution). The dimensionless flow properties downstream of the rearward Mach line are also summarized in Table 1. The results with the reference

and Chimera grids agree really well for both structured and unstructured grids. The mean values of the flow variables downstream of the rearward Mach line are approximately the same for the Chimera and reference grids, whereas the standard deviation for the Chimera grids are lower due the presence of the overlapping regions where underlying interpolations are performed. The results also agree relatively well when compared to the analytical solution. *AutoLap* is thus able to generate valid overlapping regions for the overset method.

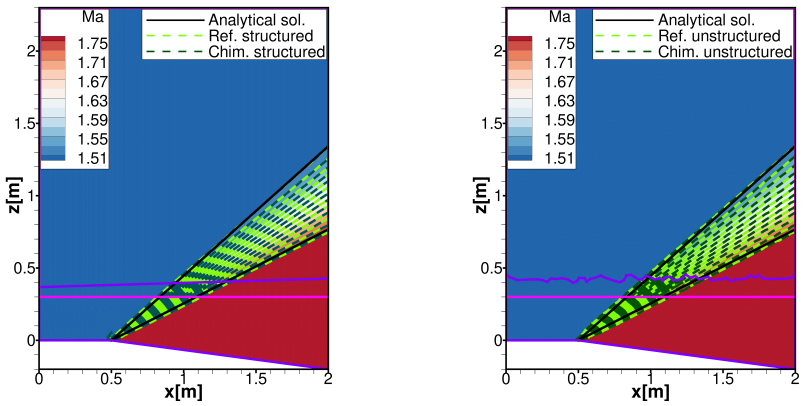

(a) Structured grid. (b) Unstructured grid.

Figure 2: Mach distribution of the steady-state expansion fan. The overlapping region of the overset meshes is located between the purple and pink lines.

Sliding Chimera boundary test case. A time dependent case, in which the chimera surface of the top grid block (depicted in pink in Fig. 1) moves in the streamwise direction is investigated here. An explicit backward Euler time-stepping scheme is applied and the grid is gradually deformed in each time step according to a sinusoidal function with a maximal amplitude of deformation of $\Delta x = 0.1\,\mathrm{m}$. Figure 3 illustrates the structured and unstructured overset grids after being deformed by the maximal amplitude. The elements on the overlapping region are, therefore, not anymore the same for both top and bottom grid blocks, and the Chimera boundaries become non-matching. Figure 4 illustrates the Mach number distribution in relation to the geodesic coordinates for the structured and unstructured overset grids and Table 2 summarizes the dimensionless flow properties downstream of the rearward Mach line for the maximal deformations. There is a good agreement between the solutions with no deformation and with the maximum deformations, even if the deformed and non-deformed meshes are not the same anymore. Hence, the developed methodology is also suitable to generate overlapping regions for overset grids used in cases where the position of the mesh nodes changes in time, i.e., cases with relative body motion as in the deployment of control surfaces.

Table 1: Summary of the dimensionless flow properties downstream of the rearward Mach line for the steady-state test case. The mean values and standard deviations of the numerical solutions are computed with regard to the grid points located downstream of the rearward Mach line.

	Ma	p	T
Analytical sol.	1.7578	0.6814	0.8962
Ref. structured	$1.7573 \pm 7.42\times10^{-3}$	$0.6822 \pm 7.68\times10^{-3}$	$0.8964 \pm 2.93\times10^{-3}$
Chim. structured	$1.7573 \pm 7.15\times10^{-3}$	$0.6821 \pm 7.40\times10^{-3}$	$0.8964 \pm 2.83\times10^{-3}$
Ref. unstructured	$1.7580 \pm 5.84\times10^{-3}$	$0.6816 \pm 6.22\times10^{-3}$	$0.8961 \pm 2.32\times10^{-3}$
Chim. unstructured	$1.7580 \pm 5.66\times10^{-3}$	$0.6816 \pm 6.02\times10^{-3}$	$0.8961 \pm 2.25\times10^{-3}$

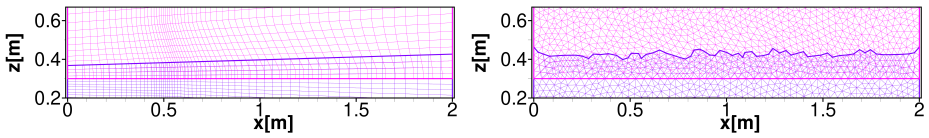

(a) Structured grid. (b) Unstructured grid.

Figure 3: Expansion fan grids after a mesh deformation of Δx. Close-up on the deformed overlapping region.

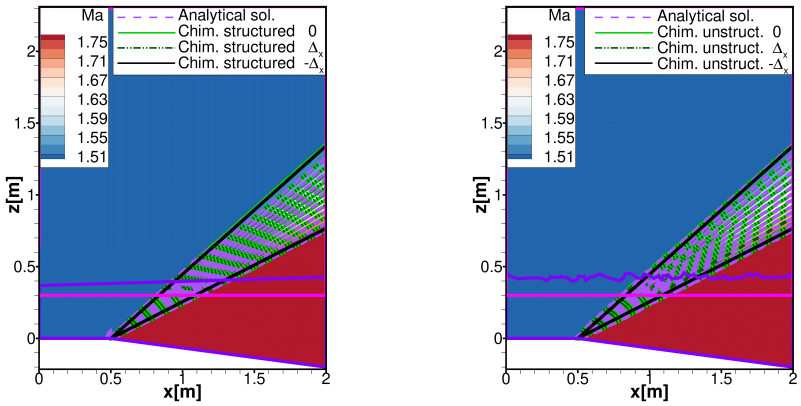

(a) Structured grid. (b) Unstructured grid.

Figure 4: Mach distribution of the expansion fan with a sliding Chimera boundary. Results are shown for the undeformed mesh, and meshes deformed by Δx and $-\Delta x$. The overlapping region is located between the purple and pink lines.

3.2 NACA0012 wing with a generic aileron

A NACA0012 finite wing with a generic aileron is studied here. The wing is characterized by a chord length of $c = 1\,\mathrm{m}$ and a spanwise length of $L_\mathrm{w} = 3.05\,\mathrm{m}$. The generic aileron is located at $0.69\,L_\mathrm{w}$ and has a spanwise length of $L_\mathrm{ail} = 0.8\,\mathrm{m}$. Gaps of $0.01\,\mathrm{m}$ separate the control and lifting surfaces.

Table 2: Summary of dimensionless flow properties downstream of the rearward Mach line for the sliding Chimera boundary test case. The mean values and standard deviations are computed with respect to the grid points located downstream of the rearward Mach line of the deformed grids.

Mesh	Ma	p	T
Chim. struct. Δx	$1.7573 \pm 7.21\times10^{-3}$	$0.6821 \pm 7.46\times10^{-3}$	$0.8964 \pm 2.85\times10^{-3}$
Chim. struct. $-\Delta x$	$1.7571 \pm 7.20\times10^{-3}$	$0.6823 \pm 7.44\times10^{-3}$	$0.8964 \pm 2.84\times10^{-3}$
Chim. unstruct. Δx	$1.7578 \pm 5.63\times10^{-3}$	$0.6817 \pm 5.97\times10^{-3}$	$0.8961 \pm 2.24\times10^{-3}$
Chim. unstruct. $-\Delta x$	$1.7578 \pm 5.80\times10^{-3}$	$0.6818 \pm 6.14\times10^{-3}$	$0.8961 \pm 2.30\times10^{-3}$

All computations are performed with an angle of attack of $\alpha = 5°$ and with the following free stream flow properties: $Ma_\infty = 0.7$, Reynolds number $Re_\infty = 7 \times 10^6$, and Prandtl number $Pr_\infty = 0.72$. The one-equation Spalart-Allmaras turbulence model in its negative form [1] is used to model the Reynolds stress tensor. Upwind spatial discretization schemes are used to initialize the simulation, switching to a second-order accurate central scheme with added matrix dissipation once a reasonable physical solution is obtained.

Here, a mesh strategy based on the creation of four grid blocks and one hole geometry is utilized, as illustrated in Fig. 5. One unstructured grid block is created for the plain wing, whereas three structured grids blocks are created for the aileron and spanwise gaps. The plain wing grid block overlaps with the structured grid blocks, so that a hole geometry is defined to blank the surface of the wing, where the aileron and the gaps are located. The gaps and aileron grid blocks are, here, structured in order to account for the vortices caused by the presence of the gaps.

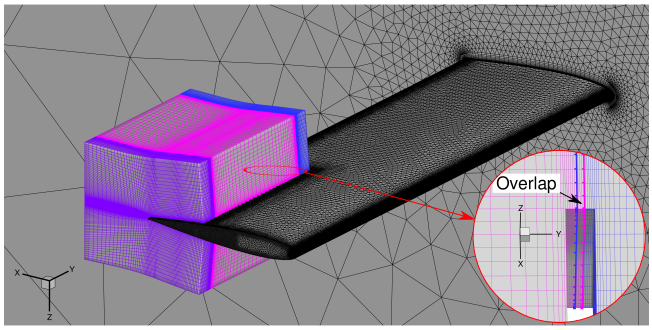

Figure 5: Mesh for the NACA wing with a generic aileron with a close-up view on the overlapping region generated by the *AutoLap* software.

Two grids composed of two-cell layer overlapping regions between the structured grid blocks are analyzed in this work: *reference Chimera* and *automatic Chimera*. For the former grid, the overlapping regions between the structured grid blocks are created directly by the mesh generation software, whereas for the latter, matching interfaces between the structured grid blocks are created

at first and are automatically extended with the methodology developed here. Both grids are characterized by the exactly same number of mesh nodes and elements: 4,046,039 mesh nodes, 8,333,501 volume elements, and 278,682 surface elements.

Here, we compute the steady flow solution for both grids with the aileron deployed by angles of $\delta = -5°$ and $\delta = -20°$ in order to ensure the functionality of *AutoLap* for moving control surfaces. During the mesh deformation process, the gap blocks (displayed in blue and purple in Fig. 5) are maintained fixed, whereas the aileron grid block (illustrated in pink in Fig. 5) is deformed. Donor cells are found for all Chimera interpolation points.

The pressure coefficient distribution and the eddy viscosity for the control surface wake (solved with the structured grid blocks) are illustrated in Fig. 6 for both meshes. The presence of the spanwise gaps leads to the formation of vortices, which influence the overall flow circulation. Thus, high-fidelity simulations of moving control surfaces must indeed consider these gaps. As the results obtained with both grids are in perfect agreement, the applicability of the *AutoLap* software for moving control surfaces is hereby proven.

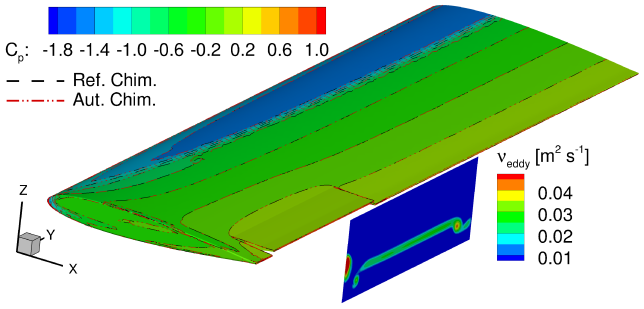

(a) Aileron deployed by $\delta = -5°$.

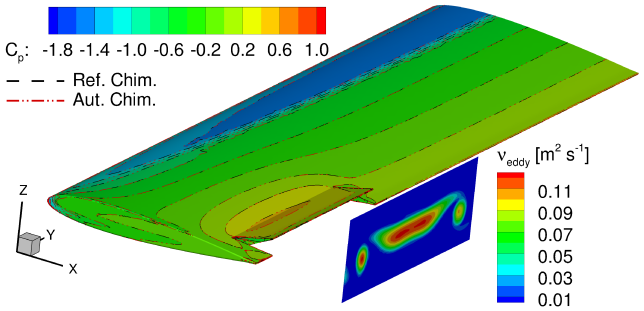

(b) Aileron deployed by $\delta = -20°$.

Figure 6: Pressure coefficient C_p and eddy viscosity ν_{eddy} distributions for the *automatic Chimera* mesh. Black dashed lines and red dashed dotted lines are the isolines of the pressure coefficient distribution for the *reference Chimera* and *automatic Chimera* grids, respectively.

4 Conclusions

The simulation of moving control surfaces is particularly challenging for realistic wing configurations. The presence of small spanwise gaps between lifting and control surfaces hampers the deployment of the control surfaces with alternatives other than mesh regeneration. Here, we focus on one approach that is successful even for these challenging configurations: the combination of the overset method with mesh deformation. The mesh generation process of overset meshes is, however, often cumbersome and time consuming. Aiming at reducing the user effort required to generate high-quality Chimera meshes, we have developed a methodology to automatically create the overlapping regions, whereby a grid with matching block interfaces is used as a starting point. This methodology has been implemented on an add-on of the DLR TAU solver, which yielded the so-called *AutoLap* software. This software is particularly interesting because it enables the extension of matching surfaces with a user-defined number of cell layers, so that even a trial-and-error approach is viable in order to generate overlapping regions within which all Chimera boundary points can be properly interpolated. *AutoLap* has been tested for the Prandtl-Meyer expansion fan with and without mesh deformation, as well as a NACA wing with a generic aileron, which was deflected by -5 and -20 degrees using a mesh deformation algorithm. Through comparisons with reference grids, the methodology developed here is verified. Thus, an important tool to assist the simulation of dynamically moving control surfaces with the combination of overset meshes and mesh deformation is provided, which can also ease the realization of high-fidelity flight maneuver simulations.

References

1. Allmaras, S.R., Johnson, F.T.: Modifications and clarifications for the implementation of the spalart-allmaras turbulence model. In: ICCFD7, pp. 1–11 (2012)
2. Blades, E.L., Marcum, D.L.: A sliding interface method for unsteady unstructured flow simulations. Int. J. Numer. Meth. Fl. **53**(3), 507–529 (2007)
3. Capsada, L.A., Heinrich, R.: Development of the DLR TAU code for modeling of control surfaces. In: DLRK 2018, p. 480018 (2018)
4. Duchon, J.: Splines minimizing rotation-invariant semi-norms in Sobolev spaces. In: W. Schempp, K. Zeller (eds.) Constructive Theory of Functions of Several Variables, pp. 85–100. Springer, Berlin, Heidelberg (1977)
5. Kroll, N., et al.: DLR project Digital-X: towards virtual aircraft design and flight testing based on high-fidelity methods. CEAS Aeronaut. J. **7**(1), 3–27 (2016)
6. Rampurawala, A.M.: Aeroelastic analysis of aircraft with control surfaces using CFD. Ph.D. thesis, University of Glasgow (2005)
7. Reimer, L., Heinrich, R.: Modeling of movable control surfaces and atmospheric effects. In: Notes on numerical fluid mechanics and multidisciplinary design: Computational Flight Testing, vol. 123, pp. 183–206. Springer Berlin Heidelberg (2013)
8. Rew, R., Davis, G.: NetCDF: an interface for scientific data access. IEEE Comput. Graph. **10**(4), 76–82 (1990)
9. Schwamborn, D., et al.: The DLR-TAU-code: recent applications in research and industry. In: ECCOMAS CFD 2006, p. 1109 (2006)